Optimal measurement constellation of the fluoroBancroft localization algorithm for position estimation in tracking confocal microscopy

Zhaolong Shen and Sean B. Andersson *

* *Department of Mechanical Engineering, Boston University, Boston, MA 02215 USA, email: {zlshen,sanderss}@bu.edu*

Abstract: The fluoroBancroft algorithm is an analytical approach that converts a collection of fluorescence intensity measurements generated by an isolated sub-diffraction limit source into an estimate with nanometer-scale precision of the source position. Based on this algorithm, we have developed a scheme for tracking single fluorescent particles in a confocal microscope. In this paper, we determine an optimal measurement constellation for the estimation algorithm. The position estimation bias and uncertainty arising from the photon counting statistics are calculated based on the assumption that the natural logarithm of a Poisson random variable with large rate can be approximated as a random variable with a Gaussian distribution. A sufficient condition for an unbiased measurement constellation and the optimal radius of a given constellation geometry with six measurements are then derived. The results are illustrated through numerical simulation.

Keywords: Estimation algorithms, Particle tracking, Parameter optimization.

1. INTRODUCTION

Single particle tracking in fluorescence microscopy is a powerful technique for investigating and understanding molecular dynamics and processes [Cheezum et al. (2001), Moerner (2007)]. Typically, this technique can be implemented with either a wide-field fluorescence image captured by a charge-coupled device (CCD) camera [Babcock et al. (2004), Murase et al. (2004)] or a position estimation algorithm based on fluorescence intensity measurements given by point photon detectors [Berglund and Mabuchi (2006), Cang et al. (2006), Wells et al. (2008)]. However, the observation time of the particle in both methods is limited by the motion of the particle in three dimensions. To overcome this limitation, feedback controllers have been designed and implemented to lock the particle inside the excitation volume of the microscope. Systems using both sample-stage actuation with piezoelectric stages and with beam-steering have been implemented. The particle trajectory is estimated from the measured displacement of the detection volume combined with estimation from the fluorescence measurements. Recent review articles about particle tracking systems can be found in [Yeung (2004), Peterman et al. (2004), Cang et al. (2008)].

In our previous work, a position estimation scheme known as the fluoroBancroft algorithm was proposed by one of the authors [Andersson (2007), Sun and Andersson (2007)] to estimate the location of a fluorescent probe in a confocal microscope by taking fluorescence intensity measurements from a collection of positions. A single particle tracking system based on this algorithm has been designed and implemented [Andersson and Sun (2009), Shen and Andersson (2009)]. The approach combines a linear quadratic Gaussian (LQG) controller with position estimation using the fluoroBancroft algorithm. Since the fluoroBancroft algorithm relies on a collection of intensity measurements obtained from different positions, the tracking algorithm sweeps the detection volume of the microscope through a "measurement constellation" that to date has been chosen in an *ad hoc* manner. Experimental results have indicated that the bias and uncertainty in the estimation procedure vary depending on the measurement constellation, motivating the need for an optimized measurement pattern. In this paper, we utilize approximations of large photon counts to analyze the statistics of the fluoroBancroft algorithm and then to determine a measurement pattern that optimizes the variance of the estimator.

This paper is organized as follows. In Section 2, a brief outline of the 3-D flouroBancroft algorithm is presented. The bias and variance of the fluoroBancroft algorithm are calculated in Section 3. An optimal measurement constellation is derived in Section 4, including a sufficient condition for an unbiased measurement constellation and the optimal relative radius for a given constellation geometry. The resulting bias and variance is illustrated through simulations presented in Section 5.

2. POSITION ESTIMATION

We give here a brief outline of the 3-D fluoroBancroft localization algorithm; details can be found in [Sun and Andersson (2007); Andersson (2007, 2008)].

The fluorescence intensity distribution of a diffraction-limited spot is given by the point spread function (PSF) of

the optical system. The resulting intensity at (x, y, z) due to a point source at (x_0, y_0, z_0) can be well approximated by a Gaussian function [Thomann et al. (2002)]:

$$I_{PSF} = me^{-\frac{(x-x_0)^2}{2\sigma_x^2} - \frac{(y-y_0)^2}{2\sigma_y^2} - \frac{(z-z_0)^2}{2\sigma_z^2}} \tag{1}$$

where σ_x, σ_y and σ_z are the widths of the PSF in the three axes respectively. By scaling the coordinates using

$$T = \begin{bmatrix} \frac{\sigma}{\sigma_x} & 0 & 0 \\ 0 & \frac{\sigma}{\sigma_y} & 0 \\ 0 & 0 & \frac{\sigma}{\sigma_z} \end{bmatrix}, \tag{2}$$

the fluorescence intensity distribution of a fluorescent particle at (x_0, y_0, z_0) can be rewritten as:

$$I_{PSF} = me^{-\frac{(x'-x_0')^2+(y'-y_0')^2+(z'-z_0')^2}{2\sigma^2}} \tag{3}$$

where

$$\begin{bmatrix} x' \\ y' \\ z' \end{bmatrix} = T \begin{bmatrix} x \\ y \\ z \end{bmatrix}, \quad \begin{bmatrix} x_0' \\ y_0' \\ z_0' \end{bmatrix} = T \begin{bmatrix} x_0 \\ y_0 \\ z_0 \end{bmatrix} \tag{4}$$

and σ is a arbitrary, nominal spread in all three axes.

Due to shot and background noise, the actual measured intensity can be modeled as

$$I = \eta_S + \eta_B \tag{5}$$

where η_S is a Poisson random variable with mean and variance equal to

$$\lambda = me^{-\frac{(x'-x_0')^2+(y'-y_0')^2+(z'-z_0')^2}{2\sigma^2}} \tag{6}$$

and η_B is a Poisson random variable with mean and variance equal to N_B. N_B can be measured experimentally and is therefore assumed to be a known constant.

The fluoroBancroft algorithm uses a collection of n measurements taken at different positions. For each measurement I_i taken at position (x_i', y_i', z_i'), define

$$\alpha_i = \frac{1}{2}({x_i'}^2 + {y_i'}^2 + {z_i'}^2) + \sigma^2 \ln(I_i - N_B) \tag{7}$$

where

$$\alpha = \begin{bmatrix} \alpha_1 \\ \vdots \\ \alpha_n \end{bmatrix}, B = \begin{bmatrix} x_1' & y_1' & z_1' & 1 \\ \vdots & \vdots & \vdots & \vdots \\ x_n' & y_n' & z_n' & 1 \end{bmatrix}, Q = \begin{bmatrix} 1 & 0 & 0 & 0 \\ 0 & 1 & 0 & 0 \\ 0 & 0 & 1 & 0 \end{bmatrix}. \tag{8}$$

The location of fluorescent probe can be estimated as

$$\begin{bmatrix} \hat{x_0} \\ \hat{y_0} \\ \hat{z_0} \end{bmatrix} = T^{-1} Q B^{\dagger} \alpha \tag{9}$$

where

$$B^{\dagger} = (B^T B)^{-1} B^T \tag{10}$$

is the Moore-Penrose generlized inverse.

3. ESTIMATION BIAS AND UNCERTAINTY

The primary noise sources in the estimation process are the shot and background noise. It is assumed that the positions (x_i', y_i', z_i') are known exactly. In practice, positioning is often achieved using a piezoelectric stage with sub-nanometer positioning resolution, justifying this assumption.

Consider first a Poisson random variable X with mean and variance equal to $\lambda_i + N_B$. Define $Z = X - N_B$. Then

$$\mathbb{E}[Z] = \lambda_i, \tag{11a}$$

$$\mathbb{V}[Z] = \lambda_i + N_B \tag{11b}$$

where $\mathbb{E}[\cdot]$ and $\mathbb{V}[\cdot]$ denote the mean and variance respectively.

Now define $Y = \ln(Z)$ and assume the rate λ_i is large enough such that Y can be approximated as a normal random variable. Then Z is a log-normal random variable with a probability density function given by

$$f_Z(z; \mu_0, \sigma_0) = \frac{1}{z\sqrt{2\pi\sigma_0^2}} e^{-\frac{(\ln(z)-\mu_0)^2}{2\sigma_0^2}}, z > 0. \tag{12}$$

According to the properties of the log-normal distribution, the mean and variance of Y can be expressed as,

$$\mu_0 = \mathbb{E}[Y] = \ln(\mathbb{E}[Z]) - \frac{1}{2}\ln\left(1 + \frac{\mathbb{V}[Z]}{(\mathbb{E}[Z])^2}\right), \tag{13a}$$

$$\sigma_0^2 = \mathbb{V}[Y] = \ln\left(1 + \frac{\mathbb{V}[Z]}{(\mathbb{E}[Z])^2}\right). \tag{13b}$$

Substituting (11) into (13) yields

$$\mathbb{E}[Y] = \ln(\lambda_i) - \frac{1}{2}\ln\left(1 + \frac{\lambda_i + N_B}{\lambda_i^2}\right), \tag{14a}$$

$$\mathbb{V}[Y] = \ln\left(1 + \frac{\lambda_i + N_B}{\lambda_i^2}\right). \tag{14b}$$

To determine the bias and variance of the estimator, consider the definition of the fluoroBancroft estimate given in (9). The only stochastic component is the vector α. According to (7) and (14), we find

$$\mathbb{E}[\alpha_i] = \frac{1}{2}\left({x_i'}^2 + {y_i'}^2 + {z_i'}^2\right) + \sigma^2\left(\ln(\lambda_i) - \frac{1}{2}\ln\left(1 + \frac{\lambda_i + N_B}{\lambda_i^2}\right)\right), \tag{15a}$$

$$\mathbb{V}[\alpha_i] = \sigma^4 \ln\left(1 + \frac{\lambda_i + N_B}{\lambda_i^2}\right). \tag{15b}$$

Define:

$$d_i = \frac{\sigma^2}{2}\ln\left(1 + \frac{\lambda_i + N_B}{\lambda_i^2}\right), \quad d = [d_1 \quad \dots \quad d_n]^T, \tag{16}$$

and

$$v_i = \sigma^4 \ln(1 + \frac{\lambda_i + N_B}{\lambda_i^2}), \quad V = \begin{bmatrix} v_1 & & \\ & \ddots & \\ & & v_n \end{bmatrix}. \tag{17}$$

Using (16) and (17) in (9), the estimation bias of the fluoroBancroft algorithm can be expressed as

$$E_b = \mathbb{E}\left[\begin{bmatrix} \hat{x_0} \\ \hat{y_0} \\ \hat{z_0} \end{bmatrix}\right] - \begin{bmatrix} x_0 \\ y_0 \\ z_0 \end{bmatrix} = -T^{-1} Q B^{\dagger} d \tag{18}$$

and the estimation uncertainty can be calculated as

$$E_u = \mathbb{V}\left[\begin{bmatrix} \hat{x_0} \\ \hat{y_0} \\ \hat{z_0} \end{bmatrix} - \begin{bmatrix} x_0 \\ y_0 \\ z_0 \end{bmatrix}\right] = T^{-1} Q B^{\dagger} V B^{\dagger T} Q^T T^{-T}. \tag{19}$$

4. OPTIMAL MEASUREMENT CONSTELLATION

To find an optimal measurement constellation, we first use (18) to derive a sufficient condition for unbiased estimation in the ideal case. Motivated by the application of tracking in confocal microscopy, we then focus on a simple six-point measurement constellation geometry with variable radius that satisfies this sufficient condition. The radius of the constellation that minimizes the estimation uncertainty is then derived according to (19).

4.1 Unbiased constellation

The values of σ_x, σ_y, and σ_z are known from the theoretical PSF of the system. The background noise intensity N_B can be determined experimentally and is thus also assumed to be known. According to (10) and (16), both $B^\dagger$ and d depend on the measurement constellation (x_i', y_i', z_i') only. Consider Proposition 2.1 in [Sun and Andersson (2007)]

Proposition 1. Let $e = (1, 1, \ldots, 1)^T$ and let A be $n \times m$ matrix. Define $B = (Ae)$. Then

$$B^\dagger e = (0 \quad 0 \quad \ldots \quad 0 \quad 1)^T.$$

□

Based on this result, if $d = d_0 e$ with d_0 a scalar constant, then according to (18), it can be shown that

$$E_b = -T^{-1} Q B^\dagger d = -d_0 T^{-1} Q B^\dagger e = 0. \tag{20}$$

Thus a sufficient condition for unbiased measurement constellation can be stated as:

Theorem 2. Consider a collection of measurement positions, or constellation, such that the expected fluorescence intensity at all measurement locations are the same. Then such a constellation yields an unbiased estimate.

□

Theorem 2 implies that unbiased estimation will be achieved if all measurements locations are on an isosurface of the fluorescence intensity. Since under the coordinate transformation defined by (2), the spreads of fluorescence intensity distribution in three axes are made identical, an unbiased constellation can be defined by a collection of measurement locations on a sphere (in the scaled coordinate system) centered on the position of the source. In practice, of course, the position of the source is unknown. Under tracking control, however, the system can be stabilized about this position leading to a unbiased steady-state estimate.

4.2 Optimal constellation

For the remainder of this paper, we choose and optimize a particular measurement constellation geometry with respect to the variance of the estimator. The constellation, illustrated in Fig. 1, is given by the six positions

$$\begin{array}{ll} (x_1', y_1', z_1') = (r, 0, 0) & (x_2', y_2', z_2') = (-r, 0, 0) \\ (x_3', y_3', z_3') = (0, r, 0) & (x_4', y_4', z_4') = (0, -r, 0) \\ (x_5', y_5', z_5') = (0, 0, r) & (x_6', y_6', z_6') = (0, 0, -r) \end{array} \tag{21}$$

centered on a sphere of radius r.

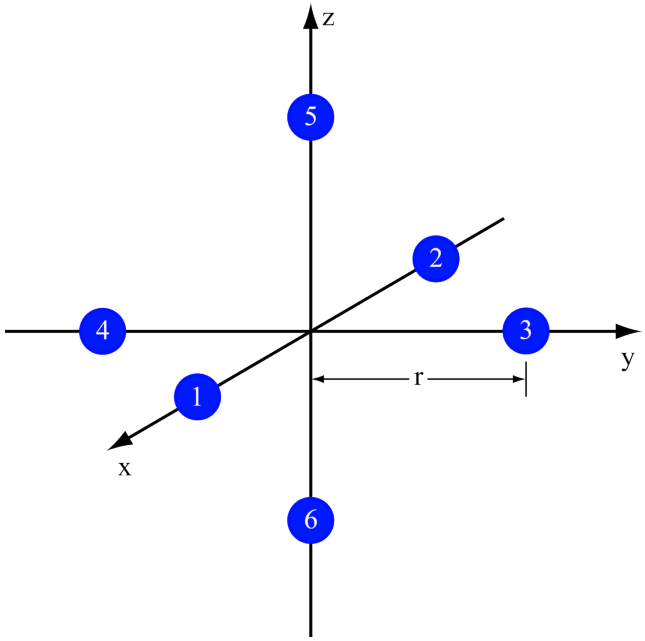

Fig. 1. The measurement constellation geometry with six measurement locations defined by a single parameter, namely the radius r.

For simplicity, define

$$r = a\sigma. \tag{22}$$

Substituting (21) into (6), we find that the rate of the intensity is given by

$$\lambda_i = m e^{-\frac{a^2}{2}},\ i = 1, \ldots, 6. \tag{23}$$

A straightforward calculation reveals that

$$B^\dagger = \begin{bmatrix} \frac{1}{2r} & -\frac{1}{2r} & 0 & 0 & 0 & 0 \\ 0 & 0 & \frac{1}{2r} & -\frac{1}{2r} & 0 & 0 \\ 0 & 0 & 0 & 0 & \frac{1}{2r} & -\frac{1}{2r} \\ \frac{1}{6} & \frac{1}{6} & \frac{1}{6} & \frac{1}{6} & \frac{1}{6} & \frac{1}{6}. \end{bmatrix}. \tag{24}$$

Assuming

$$\frac{\lambda_i + N_B}{\lambda_i^2} \ll 1, \tag{25}$$

then from (17), v_i can be approximated as

$$v_i = \frac{\sigma^4(\lambda_i + N_B)}{\lambda_i^2} = \frac{\sigma^4(m e^{-\frac{a^2}{2}} + N_B)}{m^2 e^{-a^2}}. \tag{26}$$

The estimation uncertainty (19) can be rewritten as

$$E_u = v_i Q B^\dagger \mathbb{I} B^{\dagger T} Q^T = \frac{\sigma^4(m e^{-\frac{a^2}{2}} + N_B)}{2r^2 m^2 e^{-a^2}} \mathbb{I} \tag{27}$$

where $\mathbb{I}$ is an identity matrix of the appropriate dimensions. Substituting $r = a\sigma$ into the above equation yields

$$E_u(a) = \frac{\sigma^2(m e^{-\frac{a^2}{2}} + N_B)}{2a^2 m^2 e^{-a^2}} \mathbb{I}. \tag{28}$$

To optimize this with respect to the dimensionless parameter a defining the constellation, we take the derivative of $E_u(a)$ and set it equal zero. This yields

$$\frac{a^2-2}{a^2-1}e^{-\frac{a^2}{2}} = \frac{N_B}{m}. \tag{29}$$

The peak fluorescence intensity of the particle is always greater than zero and the background noise intensity is no less than zero. Thus the right hand side of (29) is non-negative. There are thus two regimes of solutions. In the first, we have

$$0 \leq a^2 < 1 \tag{30}$$

corresponding to values of N_B/m from 2 to ∞. This regime fails to satisfy assumption (25) and is unrealistic in the sense that it represents the case where the peak fluorescence intensity of the particle is less than the background noise intensity.

In the other regime, we have

$$a^2 \geq 2. \tag{31}$$

A plot of the solution of (29) in this regime is shown in Fig. 2. Note that there are two branches. As the ratio of noise to signal goes to zero, the optimal radius goes either to ∞ or to $\sqrt{2}$. The former only makes sense if the signal level, m, itself is going to infinity. Thus in practical cases the solution branch corresponding to $\sqrt{2}$ is to be chosen.

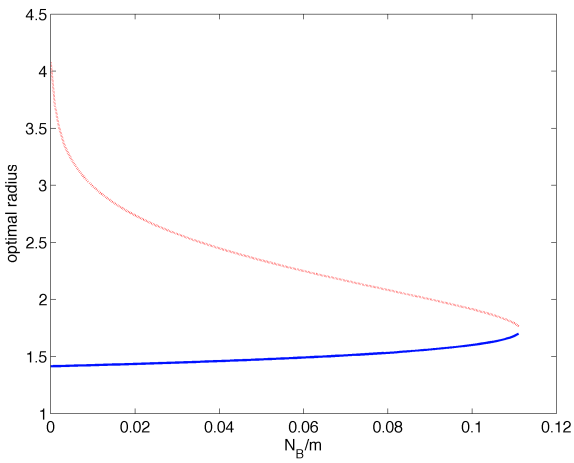

Fig. 2. The optimal radius as a function of the ratio N_B/m. The lower branch is the physically relevant one.

Note that the curve exhibits a "knee". Values of N_B/m above this point have no solution and imply a breakdown in our assumptions. We use this to characterize the bound on the relative values of m and N_B. To solve this, let $x = a^2$ and consider the equation

$$f(x) = \frac{x-2}{x-1}e^{-\frac{x}{2}}. \tag{32}$$

To find the "knee" we take the derivative of $f(x)$ and set it equal zero, yielding

$$x = 3 \quad \text{or} \quad x = 0. \tag{33}$$

The value $x = 0$ implies all the measurements are to take place at the same point. Since the fluoroBancroft algorithm requires measurements at different locations to find a solution, we ignore this case. Thus

$$a^2 = 3 \Rightarrow a = \sqrt{3}, \tag{34}$$

leading to a maximum value of $\frac{N_B}{m}$ given by

$$\frac{N_B}{m} = \frac{1}{2}e^{-\frac{3}{2}} \quad \Rightarrow \quad N_B = \frac{m}{2}e^{-\frac{3}{2}} \tag{35}$$

These results yield either a bound on the background level, given the signal level or on the signal level, given the background.

Consider now again the assumption given by (25) on the relative size of the intensity rate at the measurement locations, λ_i, and the background rate. According to (23), when $a = \sqrt{3}$, the rate is given by

$$\lambda_i = me^{-\frac{3}{2}}. \tag{36}$$

From (35) and (36), we find that at the knee

$$\lambda_i = 2N_B. \tag{37}$$

Finally, we calculate the inequality in (25) to be

$$\frac{\lambda_i + N_B}{\lambda_i^2} = \frac{1.5}{\lambda_i} \ll 1. \tag{38}$$

We therefore conclude that so long as λ_i satisfies (38), then the calculations and estimates of the estimator variance derived here are valid.

5. NUMERICAL SIMULATION

To demonstrate the feasibility of the assumptions that we made for the derivation of the optimal constellation and to illustrate our results, we ran a series of numerical simulations in Matlab to investigate the position estimation uncertainty of the fluoroBancroft algorithm and to compare the results with the theoretical predictions. In all simulations the particle was assumed to be located at the origin of the coordinate system and we set $\sigma_x = \sigma_y = \sigma_z = 0.25$ μm. In practice, the point spread function is significantly larger along the optical axis than in the optical plane. As described in Sec. 2, however, the the fluoroBancroft algorithm scales the coordinates so that the widths are the same in all directions. Our choice of equal widths, then is for convenience and without loss of generality. We selected the six-point measurement constellation defined by (21). Each intensity measurement was generated by sampling from a Poisson random variable with rate given by $\lambda_i + N_B$ where λ_i is defined in (6) and N_B was varied from 0 to 20 photons. The peak fluorescence intensity, m, was varied from 200 to 600 photons. The relative radius, a, was varied from 0.5 to 2.5. For each combination of the peak fluorescence intensity m, the background noise intensity N_B and the relative radius a, the standard deviation of the particle position estimation was calculated using 2000 iterations of the position estimation based on the 3-D fluoroBancroft algorithm. The theoretical value was calculated from (19).

In Fig. 3, we show the results of a run with the peak fluorescence intensity set to $m = 500$ photons and the background noise intensity set to $N_B = 5$ photons. The figure shows a minimum estimation uncertainty point around $a = 1.4$. The theoretical value from (29) is $a = 1.4242$. Considering the finite step size of the simulation, the simulation results matches very well with the theoretical prediction of the optimal relative radius. Similarly, the predicted and simulated variance match well. The larger

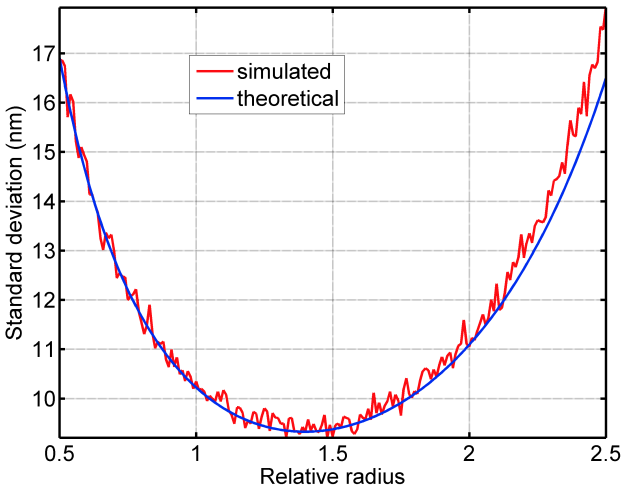

Fig. 3. The simulated and theoretical standard deviation of the position estimation of the fluorescent particle as a function of the relative radius of the measurement constellation. The peak intensity was set to $m = 500$ photons and the background noise intensity to $N_B = 5$ photons. The minimum occurs at approximately $a = 1.4$, very close to the predicted value of $a = 1.4242$.

error at high relative radius is because the measured fluorescence intensity at those values is too low to satisfy the assumptions made in the derivation.

While the theory is developed in terms of the ratio of background noise to signal, in practice it is of interest to know the separate effect of varying these two levels. In Fig. 4 we show the standard deviation of the position estimation for a range of background intensities and fixed signal level of $m = 600$ photons. In general, increasing the background noise increases the standard deviation of the fluoroBancroft estimator. It should be noted that the larger the relative radius is, the more sensitive the standard deviation of the position estimation is to the background noise. At a larger radius, the measured signal is lower. Therefore, increasing the radius can also be interpreted as decreasing the signal level. The results therefore illustrate that at low signal levels it is essential to minimize the background fluorescence. By contrast, the uncertainty is insensitive to the background rate at higher signal levels (correspondingly small values of a.)

In Fig. 5 we show the standard deviation of the position estimation for a range of signal intensities and fixed background rate. As expected, the position uncertainty decreases as the peak fluorescence intensity of the particle increases. Unlike with increasing background noise, the entire estimation uncertainty curve shifts as the signal level is increased. Moreover, as the signal level is increased, the relative improvement in the position uncertainty gets smaller. According to (27), the position estimation uncertainty goes to zero as $m \to \infty$. This is consistent with the conclusion made by Thompson in [Thompson et al. (2002)] that a fluorescent particle can be localized with any precision as long as enough photons are collected for the position estimation.

Note that the simulation curves stop at an increasingly smaller relative radius as the signal level is decreased. This

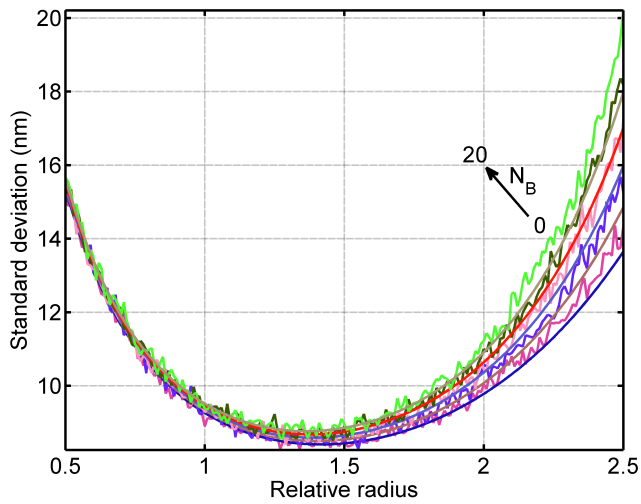

Fig. 4. The simulated and theoretical standard deviation of the position estimation of the fluorescent particle as a function of the relative radius of the measurement constellation. The peak intensity was held fixed at $m = 600$ photons and background noise intensity was varied from 0 to 20 photons.

is because at a large radius, the expected intensity from the sample drops below the background. The probability of sampling intensities lower than the background rate is then relatively high. When this happens, the fluoroBancroft algorithm fails since it relies on taking the natural logarithm of the measured intensity minus the expected background rate.

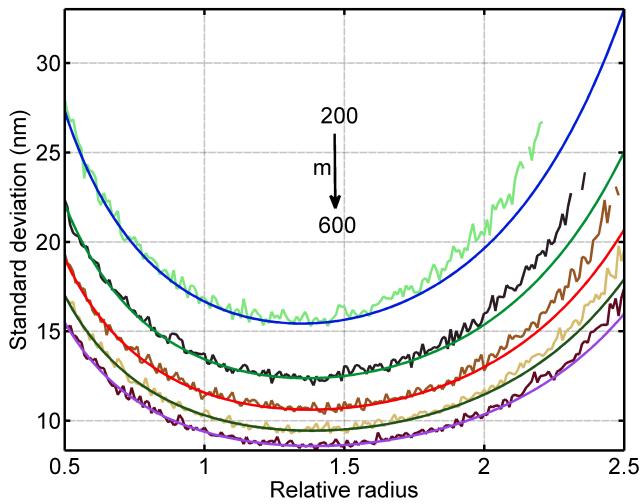

Fig. 5. The simulated and theoretical standard deviation of the position estimation of the fluorescent particle as a function of the relative radius of the measurement constellation. The background noise intensity was fixed to $N_B = 10$ photons while the peak intensity was varied from 200 to 600 photons.

6. CONCLUSION

In this paper, we considered the optimal measurement constellation problem of the fluoroBancroft localization algorithm with respect to position estimation bias and

uncertainty introduced by the photon counting statistics. We calculated the position estimation bias and uncertainty under the assumption that the natural logarithm of a Poisson random variable with a large rate can be approximated as a random variable with a Gaussian distribution. We showed that if the expected fluorescence intensity at all the measurement locations is the same, then the estimation is unbiased. The optimal measurement constellation radius was derived analytically by minimizing the position estimation uncertainty of a given unbiased constellation geometry. It was shown that if the peak fluorescence intensity is large enough, then the optimal measurement constellation radius is only determined by the ratio of the background noise intensity to the peak fluorescence intensity of the particle and that it takes the value between $\sqrt{2}\sigma$ and $\sqrt{3}\sigma$. We further showed that for these results to be meaningful, the expected fluorescence intensity from the source must be at least twice the value of the background noise.

The results depend on two major assumptions. The first is that the intensity is large enough that the distribution of the log of a Poisson-distributed random variable can be approximated by a Gaussian. The second is that the particle remains fixed during the measurement process. In practice, sub-diffraction limit estimation is used to estimate the (instantaneous) position of a moving particle. Extension of these results to the case of moving particles, to lower intensities, and for different measurement constellations is the subject of ongoing work.

ACKNOWLEDGEMENTS

This work was supported in part by the National Science Foundation through grants DBI-0649823 and CMMI-0845742.

REFERENCES

Andersson, S.B. (2007). Position estimation of fluorescent probes in a confocal microscope. In *Proceedings of the IEEE Conference on Decision and Control*, 4950–4955.

Andersson, S.B. (2008). Localization of a fluorescent source without numerical fitting. *Optics Express*, 16(23), 18714–18724.

Andersson, S.B. and Sun, T. (2009). Linear optimal control for tracking a single fluorescent particle in a confocal microscope. *Applied Physics B: Lasers and Optics*, 94(3), 403–409.

Babcock, H.P., Chen, C., and Zhuang, X. (2004). Using single-particle tracking to study nuclear trafficking of viral genes. *Biophysical Journal*, 87(4), 2749–2758.

Berglund, A.J. and Mabuchi, H. (2006). Performance bounds on single-particle tracking by fluorescence modulation. *Applied Physics B: Lasers and Optics*, 83(1), 127–133.

Cang, H., Wong, C.M., Xu, C.S., Rizvi, A.H., and Yang, H. (2006). Confocal three dimensional tracking of a single nanoparticle with concurrent spectroscopic readouts. *Applied Physics Letters*, 88(22), 223901(1–3).

Cang, H., Xu, C.S., and Yang, H. (2008). Progress in single-molecule tracking spectroscopy. *Chemical Physics Letters*, 457(4-6), 285–291.

Cheezum, M.K., Walker, W.F., and Guilford, W.H. (2001). Quantitative comparison of algorithms for tracking single fluorescent particles. *Biophysical Journal*, 81(4), 2378–2388.

Moerner, W.E. (2007). New directions in single-molecule imaging and analysis. *Proceedings of the National Academy of Sciences of the United States of America*, 104(31), 12596–12602.

Murase, K., Fujiwara, T., Umemura, Y., Suzuki, K., Iino, R., Yamashita, H., Saito, M., Murakoshi, H., Ritchie, K., and Kusumi, A. (2004). Ultrafine membrane compartments for molecular diffusion as revealed by single molecule techniques. *Biophysical Journal*, 86(6), 4075–4093. doi: http://dx.doi.org/10.1529/biophysj.103.035717.

Peterman, E.J.G., Sosa, H., and Moerner, W.E. (2004). Single-molecule fluorescence spectroscopy and microscopy of biomolecular motors. *Annual Review of Physical Chemistry*, 55, 79–96.

Shen, Z. and Andersson, S.B. (2009). LQG-based tracking of multiple fluorescent particles in two-dimensions in a confocal microscope. In *Proceedings of the American Control Conference*, 1682–1687.

Sun, T. and Andersson, S.B. (2007). Precise 3-D localization of fluorescent probes without numerical fitting. In *Proceedings of the International Conference of the IEEE Engineering in Medicine and Biology Society*, 4181–4184.

Thomann, D., Rines, D.R., Sorger, P.K., and Danuser, G. (2002). Automatic fluorescent tag detection in 3D with super-resolution: application to the analysis of chromosome movement. *Journal of Microscopy*, 208(1), 49–64.

Thompson, R.E., Larson, D.R., and Webb, W.W. (2002). Precise nanometer localization analysis for individual fluorescent probes. *Biophysical Journal*, 82(5), 2775–2783.

Wells, N.P., Lessard, G.A., and Werner, J.H. (2008). Confocal, three-dimensional tracking of individual quantum dots in high-background environments. *Analytical Chemistry*, 90(24), 9830–9834.

Yeung, E.S. (2004). Dynamics of single biomolecules in free solution. *Annual Review of Physical Chemistry*, 55, 97–126.